fluids

Article

The Influence of Two-Dimensional Temperature Modulation on Floating Droplet Dynamics

Alexander Nepomnyashchy and Ilya Simanovskii *

Department of Mathematics, Technion-Israel Institute of Technology, Haifa 32000, Israel; nepom@technion.ac.il
* Correspondence: yuri11@inter.net.il; Tel.: +972-544-378318

Abstract: We investigate the dynamics and instabilities of a droplet that floats on a liquid substrate. The substrate is cooled from below. In the framework of the slender droplet approximation and the precursor model, the problem is studied numerically. Oscillatory and stationary regimes of thermocapillary convection have been observed. The influence of a two-dimensional spatial inhomogeneity of temperature on the droplet dynamics is investigated. The two-dimensional spatial temperature inhomogeneity can suppress oscillations, changing the droplet's shape. In a definite region of parameters, the two-dimensional spatial modulation can lead to the excitation of periodic oscillations. The influence of the Biot number on the shape of the droplets is studied.

Keywords: interfacial phenomena; oscillatory instabilities; droplets

check for updates

Citation: Nepomnyashchy, A.; Simanovskii, I. The Influence of Two-Dimensional Temperature Modulation on Floating Droplet Dynamics. *Fluids* **2024**, *9*, 6. https://doi.org/10.3390/fluids9010006

Academic Editors: Manolis Gavaises and D. Andrew S. Rees

Received: 20 October 2023
Revised: 13 December 2023
Accepted: 21 December 2023
Published: 25 December 2023

1. Introduction

The motion of a viscous liquid droplet on a *solid* substrate, which contradicts the nonslip condition, has been studied extensively during the past few decades [1,2]. The exploration of the dynamic phenomena (specifically, the difference between the static and dynamic contact angles and the existence of the dynamic contact angle hysteresis) led to essential progress in the understanding of interfacial phenomena.

Droplets on a *liquid* substrate ("liquid lenses") are very important in various branches of engineering, including microfluidics [3], chemical engineering [4], environment protection [5], etc. Nevertheless, their dynamics has still attracted less attention.

The dynamics and instabilities of nonisothermal floating droplets are of special interest. Oscillatory convective motions, generated by the thermocapillary effect and buoyancy, have been observed in some experiments [6–8]. Recently, the influence of the homogeneous heating or cooling of the liquid substrate on the stability of a thin floating droplet under microgravity conditions has been studied in [9]. A number of instability modes leading to droplet oscillations, droplet decomposition or the substrate layer's rupture were revealed. The observed instabilities of droplets are reminiscent of longwave deformational instabilities in two-layer films [10].

In various applications (e.g., in microfluidic devices), it can be necessary to move a droplet in a controllable way. The simplest way to influence the dynamics of a droplet is a temperature inhomogeneity that creates a thermocapillary motion. Typically, the droplet is advected by the thermocapillary flow in a liquid layer in the direction opposite to the surface temperature gradient, but there is a contribution to the droplet velocity due to the thermocapillary stresses on the droplet interfaces and due to the shear in the substrate liquid [11]. The direction of motion can be different depending on the details of the generated convective flow [6] and the droplet shape [12]. Moreover, the direction of the flow can change periodically with time due to the laser heating of a droplet [6,7]. Experiments on droplet evaporation where the buoyancy–thermocapillary convection caused by the evaporative cooling creates hydrothermal waves [8] and leads to the droplet disintegration [13] can also be mentioned.

In the present work, the dynamics of a droplet on a liquid substrate *cooled from below* under the action of *a two-dimensional* spatial temperature modulation is studied. The results of numerical simulations carried out in the framework of the longwave approximation and the precursor model are presented. The novelty of the present investigation is as follows. We show that a two-dimensional spatial temperature modulation can significantly change the shape of the droplet and oscillation features. Specifically, the two-dimensional spatial inhomogeneity of the temperature can *suppress* oscillations, leading to the formation of steady droplets. In a definite region of parameters, the two-dimensional spatial modulation can lead to the *excitation* of the specific type of periodic oscillations. For the first time, the influence of the Biot number on the shape of the droplet is studied.

The structure of this paper is as follows. We give the formulation of the problem in Section 2. The action of the two-dimensional spatial modulation of temperature on nonlinear stationary droplets is considered in Section 3. Droplet oscillations generated by an oscillatory thermocapillary instability in the presence of two-dimensional temperature modulation are described in Section 4. The influence of gravity on the droplet dynamics is discussed in Section 5. The influence of the Biot number on the shape of droplets is considered in Section 6. Some concluding remarks are presented in Section 7.

2. Formulation of the Problem

We consider a droplet of liquid 2 that floats on the layer of liquid 1, and both are in contact with the gas phase 3 (see Figure 1). Later on, we do not consider any processes in fluid 3: at the gas/liquid interface, the viscous stresses are neglected. The heat transfer is described using the heat exchange coefficient q. The mth fluid has density ρ_m, dynamic viscosity η_m and thermal conductivity κ_m, $m = 1, 2$.

The contact angles on the triple line surrounding the droplet are determined by the balance of interfacial tensions σ_{12}, σ_{23} and σ_{13} between the corresponding fluids according to the Neumann triangle construction [14]. The droplet exists in two cases: (i) when the spreading coefficient $S = \sigma_{13} - \sigma_{12} - \sigma_{23} < 0$ (*partial wetting*); (ii) when $S > 0$ but only a small part of fluid 2 is spread between fluids 1 and 3 forming an ultrathin film (*pseudo-partial wetting*) due to the attractive interaction of those fluids through the film of fluid 2 (positive *Hamaker constant A*).

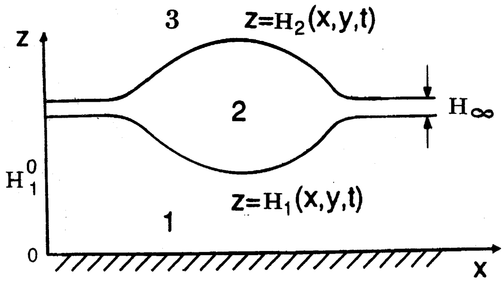

Figure 1. Geometric configuration of the region and coordinate axes.

In the present paper, we consider the thermocapillary convection in a floating droplet. The temperature of the gas phase is $T_g = const$, and the temperature of the solid substrate is a function of horizontal coordinates, $T_s = T_s(x, y)$. Assuming that the temperature differences in the system are not too large, we disregard the dependence of liquid parameters on the temperature, with only one exception: because we are interested in the investigation of the thermocapillary convection, we take into account the thermocapillary stresses proportional to derivatives of the interfacial tensions with respect to the temperature. The interfacial tension coefficients on the lower and upper surfaces of the droplet, $\sigma_1 \equiv \sigma_{12}$ and $\sigma_2 \equiv \sigma_{23}$, are assumed to be linear functions of temperature T: $\sigma_1 = \sigma_1^0 - \alpha_1 T$ and $\sigma_2 = \sigma_2^0 - \alpha_2 T$, where α_1 and α_2 are constants. It is assumed that $|\alpha_1 T| \ll \sigma_1$ and $|\alpha_2 T| \ll \sigma_2$; therefore, we disregard that dependence in the relations that contain the interfacial tensions as a whole, i.e., in the stress balances on the triple line and in the expressions for Laplace pressures.

The description of the temporal evolution of the triple line surrounding the droplet is technically difficult (see [15]). In [16], *the precursor model* was suggested for the description of a floating droplet: the interface between fluids 1 and 3 outside the droplet is replaced by an ultrathin precursor layer of fluid 2 (see Figure 1). The latter model describes the droplet on the liquid substrate as a *two-layer film*. The same equations are used in the whole region, but outside the droplet, where the top layer is ultrathin, the corresponding *disjoining pressure* is taken into account. Let us emphasize that the latter approach can be applied both in the case of pseudo-partial wetting and partial wetting, because macroscopically both cases are identical. In the present paper, we apply that approach for the description of the dynamics of a nonisothermal floating droplet.

Far from the droplet, the equilibrium thickness of layer 1 is H_1^0, and the thickness of the precursor film is H_∞. The deformable interfaces are described by equations $z = H_1(x, y, t)$ and $z = H_2(x, y, t)$. The gravity acceleration is g.

Later on, we consider a *slender* droplet, i.e., where the slopes of both droplet's interfaces are small. Also, we assume that the characteristic horizontal scale of the interface deformations is large as compared to the characteristic vertical size of the droplet and the substrate. Those assumptions allow us to apply the mathematical model governing the longwave dynamics of nonisothermal liquid layers that has been derived using the lubrication approximation [17] (see also [10,18,19]). In the framework of the longwave approach, the shapes of the interfaces $z = H_1$ and $z = H_2$ depend on the scaled horizontal coordinates $X = \epsilon x$ and $Y = \epsilon y$, $\epsilon \ll 1$, rather than on x and y. Also, it is assumed that they depend on the scaled time variable $\tau = \epsilon^2 t$. A comprehensive description of the longwave approach can be found in the review paper [20].

We present the problem in the nondimensional form using the equilibrium thickness of the lower layer, H_1^0, as the vertical length scale. The choice of the horizontal scale L^* is arbitrary [19]. We choose

$$\tau^* = \frac{\eta_1 (L^*)^4}{\sigma_1^0 (H_1^0)^3} \tag{1}$$

as a time scale and

$$p^* = \frac{\sigma_1^0 H_1^0}{(L^*)^2} \tag{2}$$

as a pressure scale.

The nondimensional parameters of the problem are as follows. We define the *local* Marangoni number as

$$M(X, Y) = \frac{\alpha_1 (T_s(X, Y) - T_g)}{\sigma_1^0} \left(\frac{L^*}{H_1^0} \right)^2, \tag{3}$$

which is *a function* of X and Y rather than a number. Also, we shall use the *mean* Marangoni number

$$\bar{M} = \frac{\alpha_1 (\bar{T}_s - T_g)}{\sigma_1^0} \left(\frac{L^*}{H_1^0} \right)^2, \tag{4}$$

where $\bar{T}_s$ is a characteristic mean temperature of the substrate.

The other nondimensional parameters of the problem are defined as follows:

$$Bi = \frac{q H_1^0}{\kappa_2} \tag{5}$$

is the Biot number, $\eta = \eta_1/\eta_2$, $\kappa = \kappa_1/\kappa_2$, $\sigma = \sigma_2^0/\sigma_1^0$, $\alpha = \alpha_2/\alpha_1$ and $\rho = \rho_2/\rho_1$.

In the framework of the lubrication approximation, the velocity and pressure fields are *enslaved* to the deformations of interfaces. The temporal evolution of those deformations is governed by the volume conservation equations [18]:

$$h_{1\tau} + \nabla \cdot \mathbf{q}_1 = 0,\ h_{2\tau} + \nabla \cdot \mathbf{q}_2 = 0, \tag{6}$$

$$\mathbf{q}_1 = f_{11}\nabla p_1 + f_{12}\nabla p_2 + \mathbf{q}_1^T,\ \mathbf{q}_2 = f_{21}\nabla p_1 + f_{22}\nabla p_2 + \mathbf{q}_2^T, \tag{7}$$

where $h_j = H_j/H_1^0$, $p_j = P_j/p^*$ and $j = 1,2$.

The expressions for pressures,

$$p_1 = -\nabla^2 h_1 - \sigma\nabla^2 h_2 + w_1(h_1,h_2), \tag{8}$$

$$p_2 = -\sigma\nabla^2 h_2 + w_2(h_1,h_2), \tag{9}$$

include the contributions of the Laplacian pressures, hydrostatic pressures and disjoining pressures. Because the thickness of liquid layer 1 is always macroscopic, we can neglect the contribution of w_1. In layer 2, we apply the following expression for the disjoining pressure:

$$w_2 = \frac{a}{(h_2-h_1)^3}\left[1 - \left(\frac{h_\infty}{h_2-h_1}\right)^3\right], \tag{10}$$

where a is the nondimensional Hamaker constant, which is related to the dimensional Hamaker constant A as follows:

$$a = \frac{A(L^*)^2}{6\pi\sigma_1^0(H_1^0)^4}, \tag{11}$$

and $h_\infty = H_\infty/H_1^0$ (for details, see [16,21]).

The expressions for mobilities f_{ij}, $i,j = 1,2$, are

$$f_{11} = -\frac{1}{3}h_1^3,\ f_{12} = -\frac{1}{2}h_1^2(h_2-h_1),$$

$$f_{21} = \frac{1}{6}h_1^3 - \frac{1}{2}h_1^2h_2,\ f_{22} = (h_2-h_1)\left[h_1^2\left(\frac{1}{2}-\frac{\eta}{3}\right) + h_1h_2\left(-1+\frac{2\eta}{3}\right) - \frac{\eta}{3}h_2^2\right].$$

The nondimensional expressions for the rates of the thermocapillary flows are

$$\mathbf{q}_1^T = -\frac{h_1^2}{2}\nabla\{M[1+d(\alpha\kappa - Bih_1)]\}, \tag{12}$$

$$\mathbf{q}_2^T = -\frac{\eta\alpha\kappa}{2}h_2^2\nabla(Md) +$$

$$\frac{(2h_2-h_1)h_1}{2}\nabla\{M[-1+Bih_1d - \alpha\kappa(1-\eta)d]\}, \tag{13}$$

where

$$d = [\kappa + Bi(1-\kappa)h_1 + Bi\kappa h_2]^{-1}. \tag{14}$$

Note that in the absence of gravity, a liquid layer with a deformable interface is subject to a monotonic Marangoni instability for arbitrary $\bar{M} > 0$, i.e., by any heating from below [22]. That instability is not saturable, and it leads to the rupture of the substrate layer. The temperature disturbance caused by the droplet acts as “a seed” of instability. Therefore, in the presence of the temperature gradient, one can expect the existence of a stable configuration containing a droplet on a layer flat on the infinity only if $\bar{M} < 0$, i.e., by cooling from below.

In the present work, we consider nonlinear regimes of the thermocapillary convection in the case of a spatially periodic temperature modulation of the local Marangoni number,

$$M(X,Y) = \bar{M}\left(1 + \delta_X \sin\frac{2\pi X}{L} + \delta_Y \sin\frac{2\pi Y}{L}\right) = \bar{M} - \Delta_X \sin\frac{2\pi X}{L} - \Delta_Y \sin\frac{2\pi Y}{L}, \quad (15)$$

where $\bar{M} < 0$, $\delta_X \geq 0$, $\Delta_X = |\bar{M}|\delta_X \geq 0$, $\delta_Y \geq 0$ and $\Delta_Y = |\bar{M}|\delta_Y \geq 0$. Note that the change in the sign of δ_X or δ_Y is obtained by a translation $X \to X + L/2$ or $Y \to Y + L/2$, correspondingly. Because of the symmetry of the problem with respect to the transformations $X \to Y$ and $Y \to X$, it is sufficient to consider the case $\delta_Y \geq \delta_X$.

The problem governed by Equations (6)–(10) and (12)–(15) has been solved numerically with some initial conditions. The evolution equations were discretized using central differences for spatial derivatives and solved using an explicit scheme. Periodic boundary conditions have been applied on the boundaries of the computational region $L \times L$.

The computations have been performed in the region $L \times L = 240 \times 240$ using the grid 80×80. Some additional simulations on the grids 100×100 and 120×120 did not reveal any qualitative changes.

Computations have been performed for the system of fluorinert FC70 (liquid 1) and silicon oil 10 (liquid 2). This system was used in microgravity experiments (see, e.g., [23]). We applied the following set of liquid parameters that was formerly used in simulations of the thermocapillary instability in two-layer systems [19]: $\eta = 3.04$, $\kappa = 0.522$, $\alpha = 2$, $\rho = 0.482$, $\sigma = 2.6$. $h_- = 1.02$, $h_+ = 1$, $R = 60$, $h_\infty = 0.01$, $Bo = 0$ and $Bi = 20$. The value of a_2 is chosen equal to 3×10^{-6} (see [9]).

3. Manipulation by a Stationary Droplet

In this section, we describe the shape of a stationary droplet in the limit of large τ.

3.1. The Case of Axisymmetric Initial Conditions

It is known that in the absence of gravity and the thermocapillary effect, both interfaces of an equilibrium droplet are spherical caps. The exact formulas that follow from the balance of interfacial tensions on the triple line are given in [24]. In the longwave limit, these interfaces become paraboloids with constant values of $d^2h_1/dr^2 > 0$ and $d^2h_2/dr^2 < 0$, where r is the radial coordinate. When a temperature gradient across the substrate layer is applied, the temperature on both droplet interfaces becomes inhomogeneous; therefore, the thermocapillary convection is developed both in the droplet and in the substrate. If the initial conditions with an axisymmetric drop shape are applied and $\Delta_X = \Delta_Y = 0$, for sufficiently small values of $|\bar{M}|$ the droplet is stationary and axisymmetric in the limit $\tau \to \infty$. The shapes of isolines for $h_1(X,Y)$ and $h_2(X,Y)$, which are determined by equations $\mathbf{q}_1 = 0$ and $\mathbf{q}_2 = 0$, look perfectly circular, despite the violation of the rotational symmetry by the periodic boundary conditions [9]. Note that in contradistinction to the case of an isothermal droplet, both d^2h_1/dr^2 and d^2h_2/dr^2 are negative, except the vicinity of the triple line. Indeed, when the terms $\mathbf{q}_1^T$ and $\mathbf{q}_2^T$ caused by the inhomogeneities of the interfacial temperatures are dominant in the expressions (7) for flow rates, the system tends to minimize those inhomogeneities. The temperature of the interface between the substrate and the droplet is nearly constant when the ratio $h_2(r)/h_1(r)$ is nearly constant.

Let us take the steady round droplet [9] ($\bar{M} = -2$; $\Delta_X = \Delta_Y = 0$) as the initial condition and consider its evolution under the action of two-dimensional temperature modulation ($\bar{M} = -2$; $\Delta_X = \Delta_Y = 0.1$). In the case $\Delta_X = \Delta_Y \equiv \Delta$, the Marangoni number field (15) can be written as

$$M(X,Y) = \bar{M} + \tilde{M}(X,Y),\ \tilde{M}(X,Y) = -2\Delta \sin\frac{\pi(X+Y)}{L} \cos\frac{\pi(X-Y)}{L}.$$

Thus, the substrate temperature inhomogeneity has the shape of a square pattern. The function $\tilde{M}(X,Y)$ is symmetric with respect to axes $X = L/4$, $X = 3L/4$, $Y = L/4$ and

$Y = 3L/4$. It changes its sign on the lines $Y = L - X$ and $Y = X \pm L/2$. Near the diagonal $Y = X$, it is negative for $X < L/2$ and positive for $X > L/2$. Under the action of the thermocapillary stresses, the liquid in the droplet moves slowly towards the region $X < L/2, Y < L/2$, changing its shape and height. The intermediate stages of the evolution of the initially round droplet are presented in Figure 2. A change in the droplet's shape is visible between Figure 2a,c. At $\tau \geq 200{,}000$, the equilibration takes place. Finally, we obtain the steady droplet with the maximum, shifted along the axis $Y = X$ to the region $X < L/2$, where the local value of $|M|$ is higher (i.e., into the cooler part of the region). Figure 3 shows a snapshot of the fields of (a) $h_2(X, Y, \tau)$ and (b) $h_1(X, Y, \tau)$ at the equilibrium stage. The droplet is not round anymore, but it keeps the symmetry with respect to the axis $Y = X$.

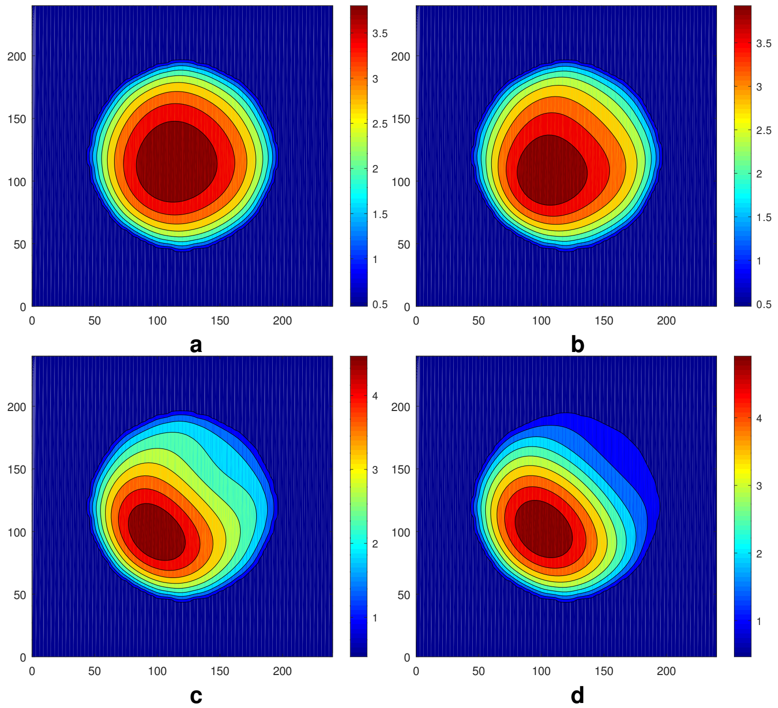

Figure 2. The fields of $h_2(X, Y, \tau)$ for $\bar{M} = -2$, $\Delta_X = \Delta_Y = 0.1$, $Bo = 0$ and $Bi = 20$: (**a**) $\tau = 750$; (**b**) $\tau = 1500$; (**c**) $\tau = 4500$; (**d**) τ = 10,000.

Let us consider now the action of an increased temperature modulation, $\Delta_X = \Delta_Y = 0.5$, on the initially round steady droplet. The intermediate states of the evolution of the initially round droplet under the action of two-dimensional temperature modulation are presented in Figure 4. As in the previous case, in the early stages the liquid in the droplet moves to the left bottom part of the computational region (Figure 4a,b). A visible change in the droplet's shape takes place between Figure 4a,c. One can see the division of the droplet and the creation of two satellites that are symmetric with respect to the axes $Y = X$ (see Figure 4e,f). With an increase in time (at $\tau \geq 100{,}000$), the further evolution of the droplet and the equilibration takes place. Finally, we obtain a steady droplet with the maximum significantly shifted along the axis $Y = X$ to the region $X < L/2$. A snapshot of the fields of (a) $h_2(X, Y, \tau)$ and (b) $h_1(X, Y, \tau)$ at the equilibrium stage is shown in Figure 5 and the corresponding shapes of interfaces are presented in Figure 6. The droplet keeps the symmetry with respect to the axis $Y = X$. One can see that the droplet becomes much shorter in the direction of the axis $Y = X$ (see Figure 5). Let us note that the droplet is significantly higher than that obtained in the case $\Delta_X = \Delta_Y = 0.1$ (cf. Figures 3 and 5).

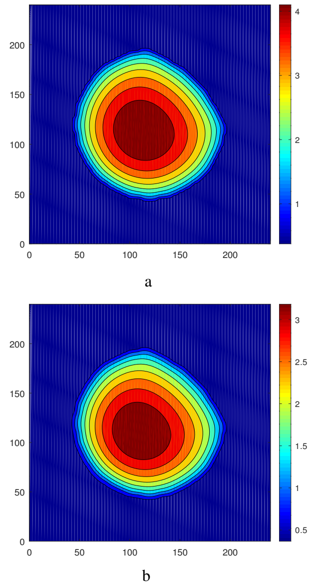

Figure 3. A snapshot of the fields of $h_2(X,Y,\tau)$ and $h_1(X,Y,\tau)$ for $\bar{M} = -2$, $\Delta_X = \Delta_Y = 0.1$, $Bo = 0$, $Bi = 20$ and $\tau = 1 \times 10^6$.

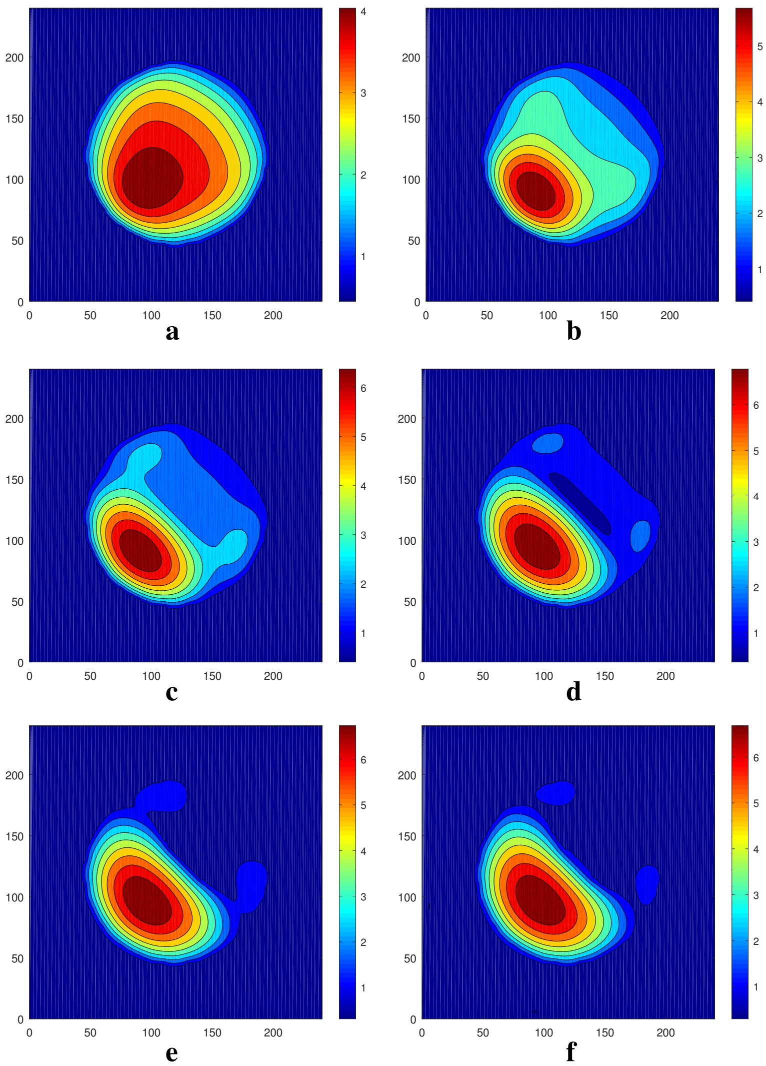

Figure 4. The fields of $h_2(X,Y,\tau)$ for $\bar{M} = -2$, $\Delta_X = \Delta_Y = 0.5$, $Bo = 0$ and $Bi = 20$: (**a**) $\tau = 500$; (**b**) $\tau = 1500$; (**c**) $\tau = 2500$; (**d**) $\tau = 5000$; (**e**) $\tau = 8000$ (**f**) $\tau = 9500$.

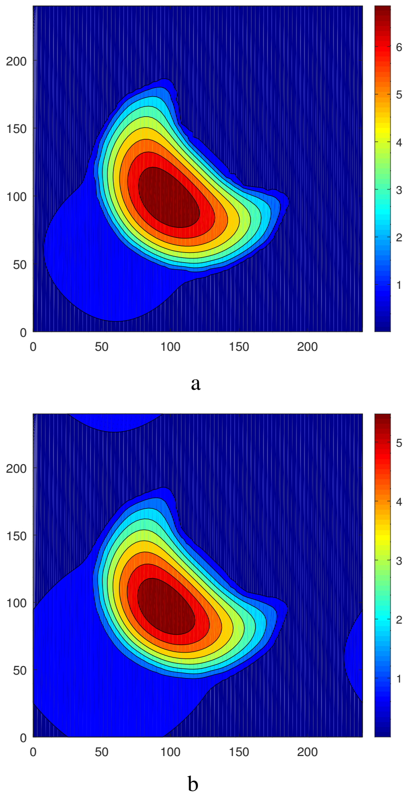

Figure 5. A snapshot of the fields of $h_2(X, Y, \tau)$ and $h_1(X, Y, \tau)$ for $\bar{M} = -2$, $\Delta_X = \Delta_Y = 0.5$, $Bo = 0$, $Bi = 20$ and $\tau = 1 \times 10^6$.

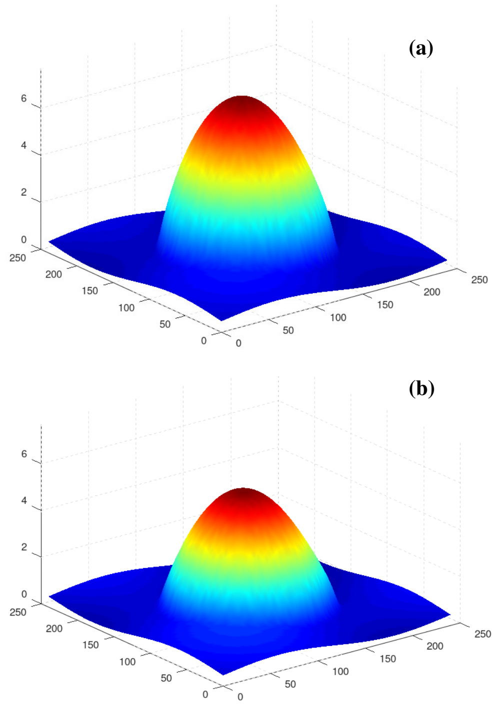

Figure 6. The shapes of (**a**) $h_2(X, Y, \tau)$ and (**b**) $h_1(X, Y, \tau)$ for $\bar{M} = -2$, $\Delta_X = \Delta_Y = 0.5$, $Bo = 0$, $Bi = 20$ and $\tau = 1 \times 10^6$.

Under the action of the asymmetric field $M(X, Y)$ ($\Delta_X = 0.1; \Delta_Y = 0.5$) on the steady round droplet, the symmetry of the initially round droplet is broken. A snapshot of the fields of (a) $h_2(X, Y, \tau)$ and (b) $h_1(X, Y, \tau)$ is shown in Figure 7, and the shapes of the interfaces are presented in Figure 8. Now, there is no symmetry with respect to the axis $Y = X$ (cf. Figures 3 and 7).

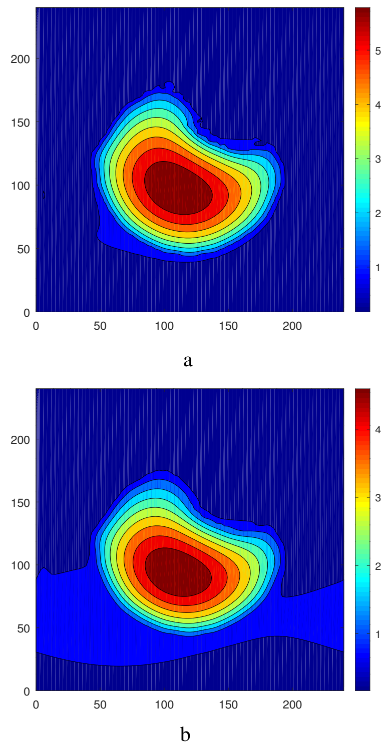

Figure 7. A snapshot of the fields of $h_2(X, Y, \tau)$ and $h_1(X, Y, \tau)$ for $\bar{M} = -2$, $\Delta_X = 0.1, \Delta_Y = 0.5$, $Bo = 0$, $Bi = 20$ and $\tau = 1 \times 10^6$.

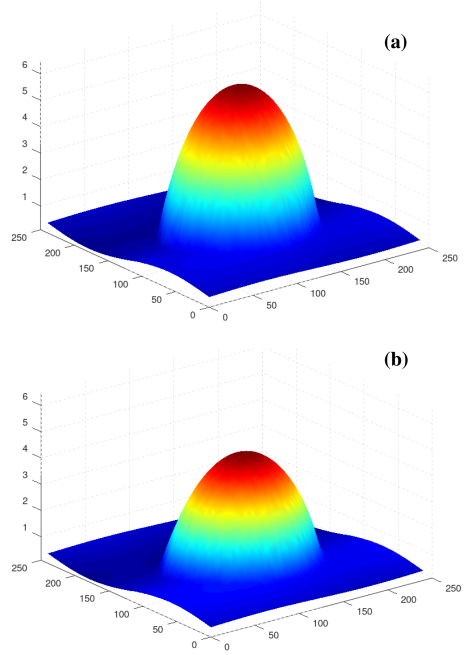

Figure 8. The shapes of (**a**) $h_2(X, Y, \tau)$ and (**b**) $h_1(X, Y, \tau)$ for $\bar{M} = -2$, $\Delta_X = 0.1, \Delta_Y = 0.5$, $Bo = 0$, $Bi = 20$ and $\tau = 1 \times 10^6$.

3.2. The Case of Nonaxisymmetric Initial Conditions

Let us take now the steady droplet with the maximum, shifted to the left part of the computational region (see Figure 3 in [25]), as the initial conditions and consider its evolution under the action of two-dimensional temperature modulation ($\bar{M} = -2$; $\Delta_X = \Delta_Y = 0.1$). Despite the symmetry of the spatial temperature modulation, we obtain an asymmetric steady state. A snapshot of the fields of (a) $h_2(X, Y, \tau)$ and (b) $h_1(X, Y, \tau)$ is shown in Figure 9, and the shapes of the interfaces are presented in Figure 10.

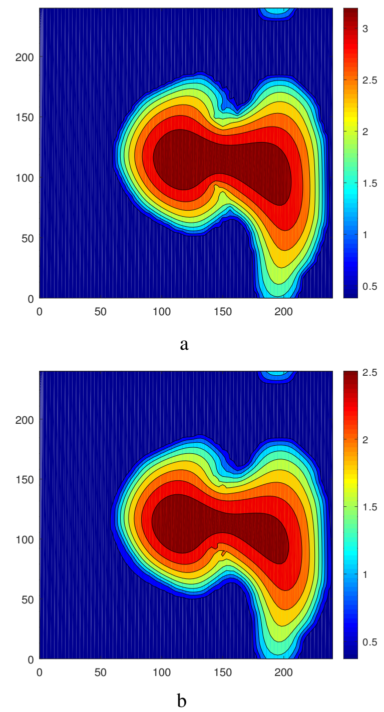

Figure 9. A snapshot of the fields of (**a**) $h_2(X, Y, \tau)$ and (**b**) $h_1(X, Y, \tau)$ for $\bar{M} = -2$, $\Delta_X = \Delta_Y = 0.1$, $Bo = 0$, $Bi = 20$ and $\tau = 1 \times 10^6$.

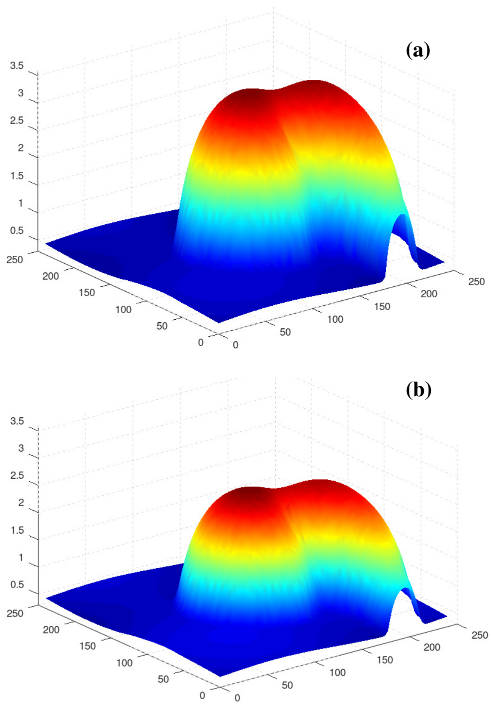

Figure 10. The shapes of (**a**) $h_2(X, Y, \tau)$ and (**b**) $h_1(X, Y, \tau)$ for $\bar{M} = -2$, $\Delta_X = \Delta_Y = 0.1$, $Bo = 0$, $Bi = 20$ and $\tau = 1 \times 10^6$.

4. Droplet Oscillations

It has been shown in [9] that in the case of a homogeneous cooling from below, the droplet becomes oscillatory unstable with an increase in $\bar{M}$ (see Figure 11). That instability is similar to that formerly found in a system of two flat liquid layers [10]. Let us note that oscillatory Marangoni instabilities for cooling from below have also been observed in some other problems (see [26]).

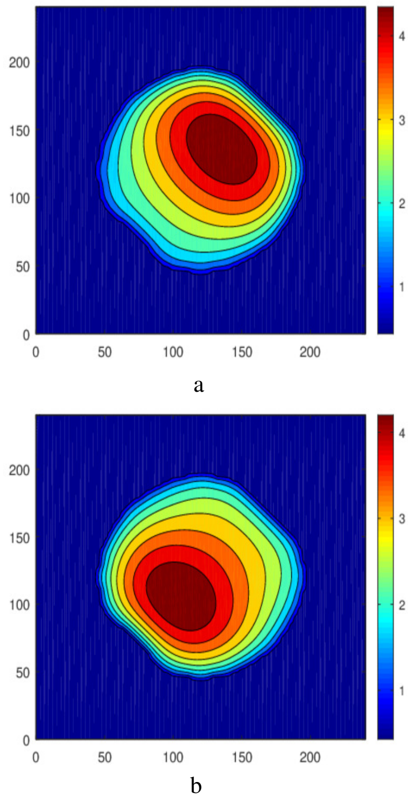

Figure 11. A snapshot of the fields of $h_2(X, Y, \tau)$ for $\bar{M} = -2.5$, $Bi = 20$ and $\Delta_X = \Delta_Y = 0$: (**a**) $\tau = 7 \times 10^5$; (**b**) $\tau = 7.15 \times 10^5$.

In the course of oscillations, the droplet keeps the symmetry with respect to the axis $Y = X$. Also, the oscillations are characterized by the symmetry

$$h_m(X, Y, \tau + T/2) = h_m(L - Y, L - X, \tau), \ m = 1, 2, \tag{16}$$

where T is the period of oscillations. In other words, after the half-period, the shape of the droplet is reflected with respect to the axis $X + Y = L$. Therefore, the quantities

$$h_{max,m}(\tau) = \max h_m(X, Y, \tau)$$

and

$$h_{min,m}(\tau) = \min h_m(X, Y, \tau)$$

are periodic in time with the period $T/2$. The temporal evolution of $h_{max,1}$ and $h_{max,2}$ is shown in Figure 12.

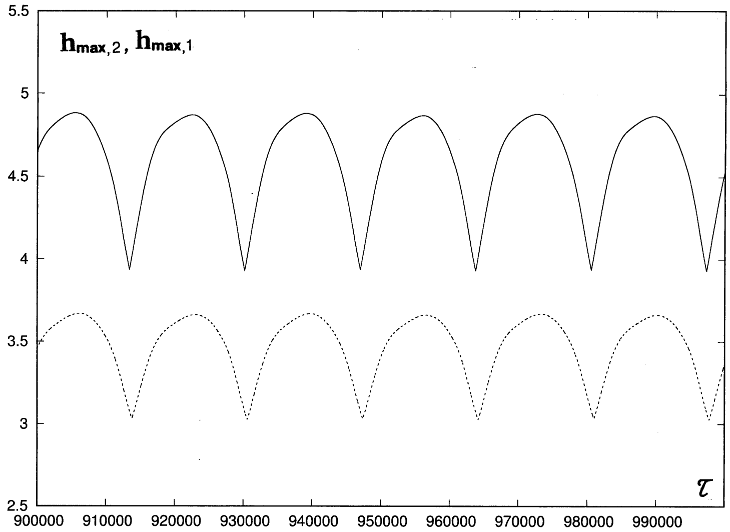

Figure 12. The oscillations of $h_{max,2}(\tau)$ (solid line) and $h_{max,1}(\tau)$ (dashed line) for $\bar{M} = -2.5$ and $Bi = 20$.

Below, we discuss the influence of the substrate temperature modulation on the oscillatory regime.

4.1. Suppression of Oscillations

Let us take the oscillatory droplet (see Figures 11 and 12) ($\bar{M} = -2.5$; $\Delta_X = \Delta_Y = 0$) as the initial conditions and consider its evolution under the action of two-dimensional spatial temperature modulation ($\bar{M} = -2.5$; $\Delta_X = \Delta_Y = 0.1$). Under the action of the symmetric field $M(X,Y)$, the oscillations are suppressed and the steady state develops in the system. The transient process from the periodic oscillations to the steady droplet is shown in Figure 13, and the intermediate stages of the evolution at different instants of time are presented in Figure 14. One can see that the symmetry of the droplet is broken. Finally, a steady *asymmetric* droplet is observed in the system. A snapshot of the fields of (a) $h_2(X,Y,\tau)$ and (b) $h_1(X,Y,\tau)$ at the equilibrium stage is shown in Figure 15, and the corresponding shapes of the interfaces are presented in Figure 16.

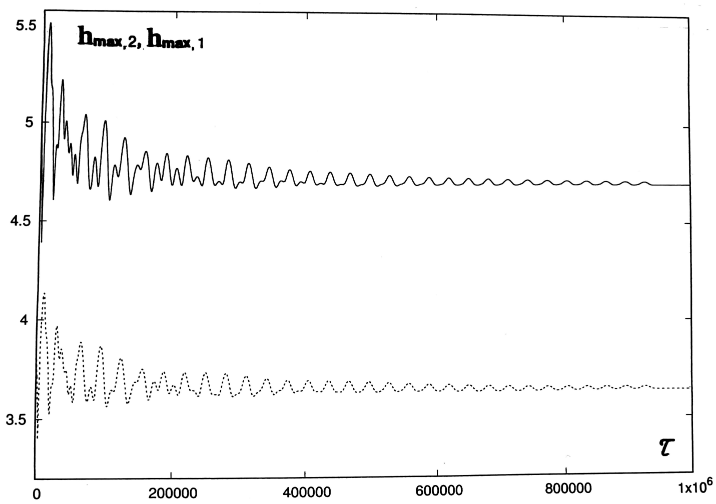

Figure 13. The oscillations of $h_{max,2}(\tau)$ (solid line) and $h_{max,1}(\tau)$ (dashed line) for $\bar{M} = -2.5$, $\Delta_X = \Delta_Y = 0.1$, $Bo = 0$ and $Bi = 20$.

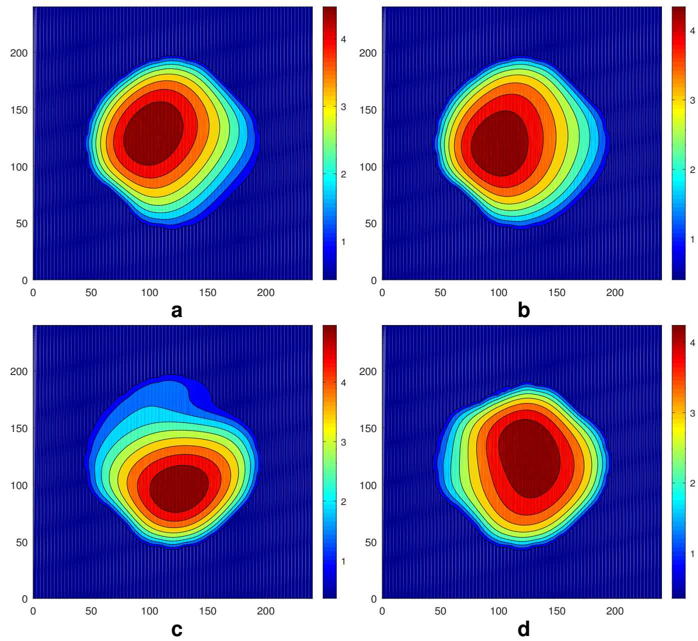

Figure 14. The fields of $h_2(X, Y, \tau)$ for $\bar{M} = -2.5$, $\Delta_X = \Delta_Y = 0.1$, $Bo = 0$ and $Bi = 20$: (**a**) $\tau = 500$; (**b**) $\tau = 1500$; (**c**) τ = 10,000; (**d**) τ = 20,000.

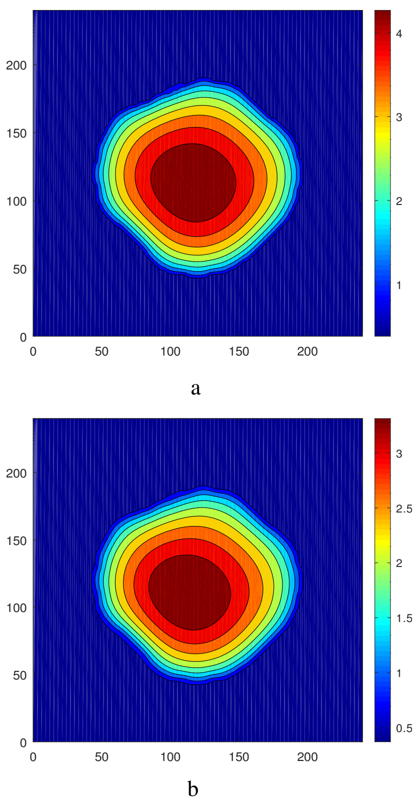

Figure 15. A snapshot of the fields of (**a**) $h_2(X, Y, \tau)$ and (**b**) $h_1(X, Y, \tau)$ for $\bar{M} = -2.5$, $\Delta_X = \Delta_Y = 0.1$, $Bo = 0$, $Bi = 20$ and $\tau = 1 \times 10^6$.

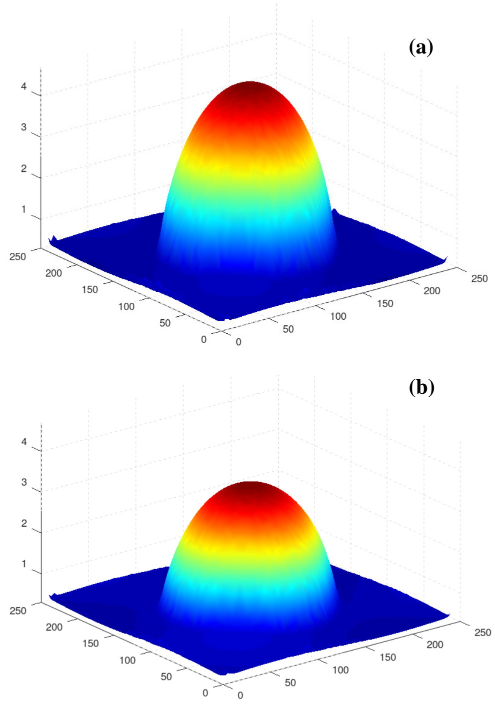

Figure 16. The shapes of (**a**) $h_2(X, Y, \tau)$ and (**b**) $h_1(X, Y, \tau)$ for $\bar{M} = -2.5$, $\Delta_X = \Delta_Y = 0.1$, $Bo = 0$, $Bi = 20$ and $\tau = 1 \times 10^6$.

Let us consider the influence of asymmetric field $M(X, Y)$ on the oscillatory regime presented in Figures 11 and 12—we take $\Delta_X = 0.1$ and $\Delta_Y = 0.5$ ($M = -2.5$). In this case, the oscillations are also suppressed and the asymmetric steady droplet develops in the system. A snapshot of the fields of (a) $h_2(X, Y, \tau)$ and (b) $h_1(X, Y, \tau)$ is presented in Figure 17, and the shapes of the interfaces are shown in Figure 18. The sharp corners in Figure 18 present the connection of the droplet with the neighbor droplet and are created by the crossing of the interfaces with the plane $X = 0$, which cuts the droplet. One can see that the shape of the droplet is rather smooth.

4.2. Excitation of Oscillations

Surprisingly, we observed *an excitation* of oscillations for $\bar{M} = -2$, i.e., in the case where in the absence of modulation the round droplet is stable, when we apply an asymmetric field $M(X, Y)$ ($\Delta_X = 0.1$, $\Delta_Y = 0.5$) on the asymmetric steady droplet with the maximum, shifted to the left part of the computational region (see Figure 3 in [25]). In this case, periodic oscillations with essentially different adjacent maxima develop in the system (see Figure 19); the period of oscillations T = 69,420. Snapshots of the fields $h_2(X, Y, \tau)$ at different instants of time are presented in Figure 20. The small and big maxima of $h_{max,j}(\tau)$, $j = 1, 2$, correspond to different spatial points. Let us note that because the different maxima are in the points with different values of $M(X, Y)$, there is no reason for them to be equal. Since we consider the region with periodic boundary conditions, one can see the appearance of a finger that meets the fingers of the neighbor drops at the boundary of the computational region. The combination and the recombination of the droplet with its neighbors could be the origin of the oscillations. The shapes of interfaces, corresponding to Figure 20b, are shown in Figure 21. A diagram of the regimes in the plane (δ_X, δ_Y) for $\bar{M} = -2$ is presented in Figure 22. One can see that bistability takes place at several points.

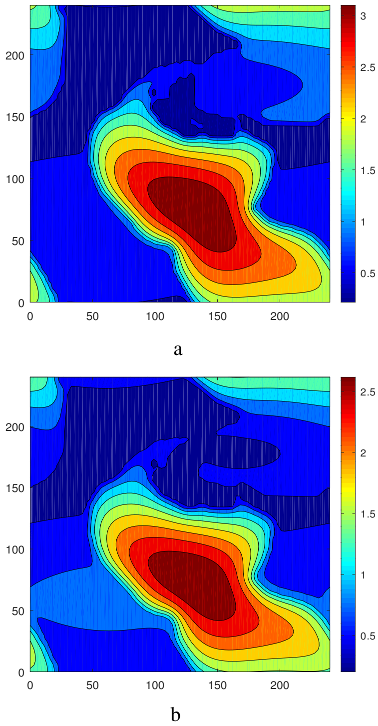

Figure 17. A snapshot of the fields of (**a**) $h_2(X,Y,\tau)$ and (**b**) $h_1(X,Y,\tau)$ for $\bar{M} = -2.5$, $\Delta_X = 0.1$, $\Delta_Y = 0.5$, $Bo = 0$, $Bi = 20$ and $\tau = 1 \cdot 10^6$.

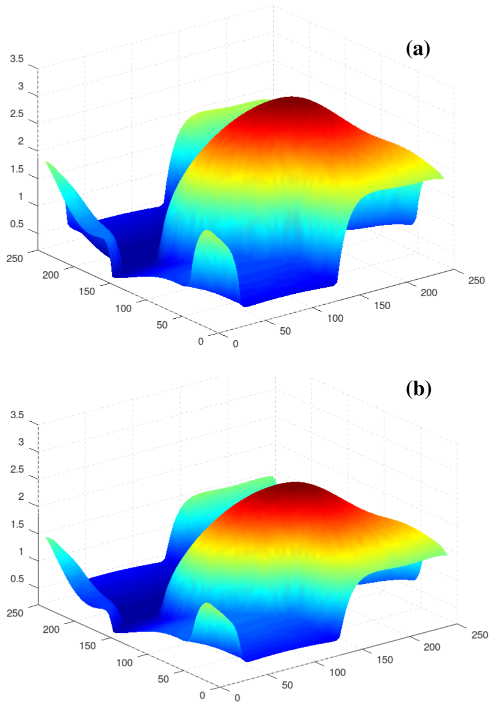

Figure 18. The shapes of (**a**) $h_2(X,Y,\tau)$ and (**b**) $h_1(X,Y,\tau)$ for $\bar{M} = -2.5$, $\Delta_X = 0.1$, $\Delta_Y = 0.5$, $Bo = 0$, $Bi = 20$ and $\tau = 1 \times 10^6$.

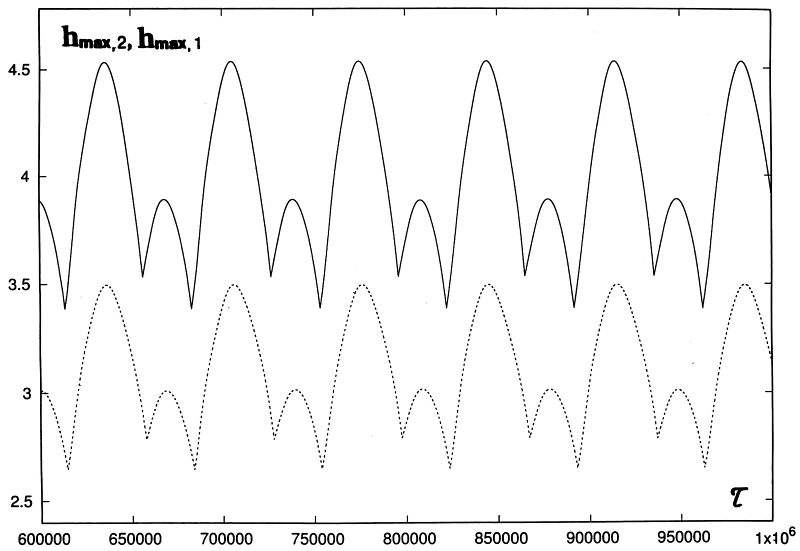

Figure 19. The oscillations of $h_{max,2}(\tau)$ (solid line) and $h_{max,1}(\tau)$ (dashed line) for $\bar{M} = -2$, $\Delta_X = 0.1$, $\Delta_Y = 0.25$, $Bo = 0$ and $Bi = 20$.

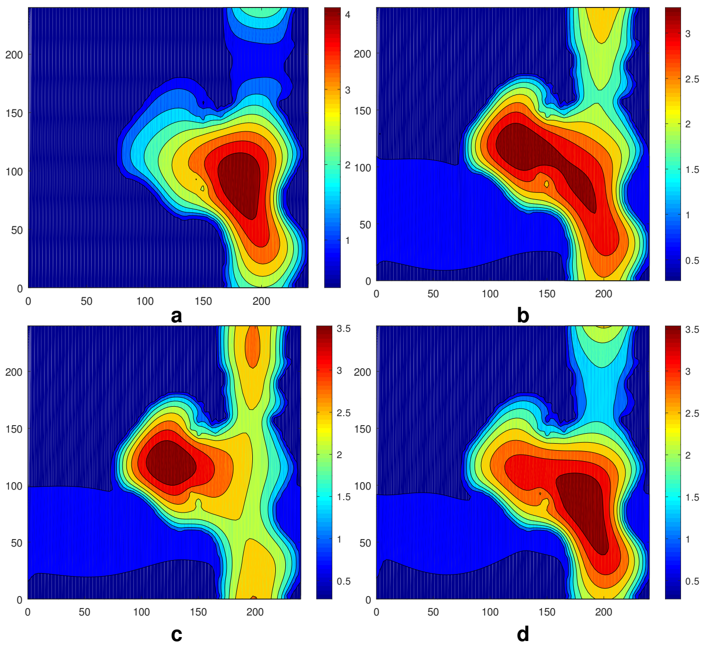

Figure 20. The fields of $h_2(X, Y, \tau)$ for $\bar{M} = -2$, $\Delta_X = 0.1, \Delta_Y = 0.25$, $Bo = 0$ and $Bi = 20$: (**a**) $\tau = 9.15 \times 10^5$; (**b**) $\tau = 9.3 \times 10^5$; (**c**) $\tau = 9.35 \times 10^5$; (**d**) $\tau = 9.5 \times 10^5$.

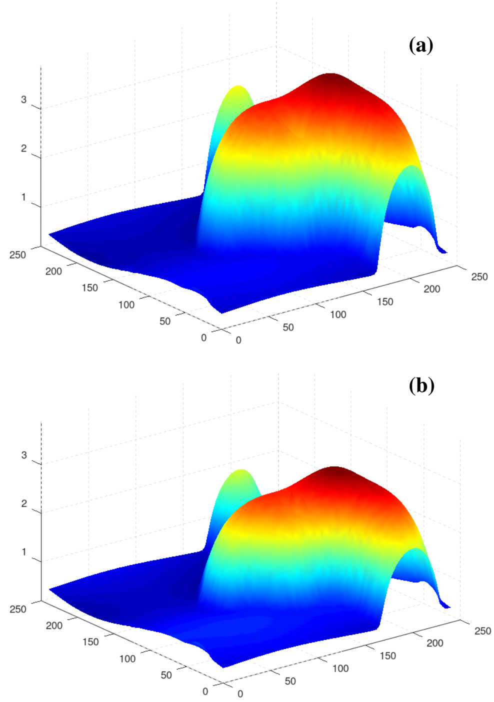

Figure 21. The shapes of (**a**) $h_2(X, Y, \tau)$ and (**b**) $h_1(X, Y, \tau)$ for $\bar{M} = -2$, $\Delta_X = 0.1$, $\Delta_Y = 0.25$, $Bo = 0$, $Bi = 20$ and $\tau = 9.3 \times 10^5$.

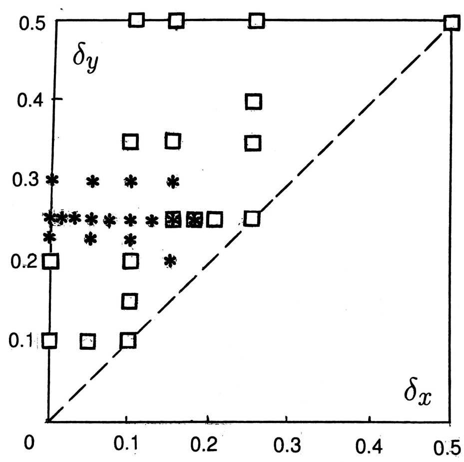

Figure 22. Diagram of regimes on the plane (δ_X, δ_Y) for $M = -2$, $Bo = 0$ and $Bi = 20$: empty square, stationary pattern; asterisk, oscillatory flow.

Let us take the oscillatory flow presented in Figures 19 and 20a as the initial condition and consider its evolution at the larger values of $|\bar{M}|$. With an increase in $|\bar{M}|$, periodic oscillations with different adjacent maxima become of a rather complex form; the amplitude of oscillations grows and the period of oscillations decreases (cf. Figure 23 ($T = 52{,}940$) and Figure 19 ($T = 69{,}420$)). At $\bar{M} \leq -2.92$, quasiperiodic oscillations develop in the system (see Figure 24).

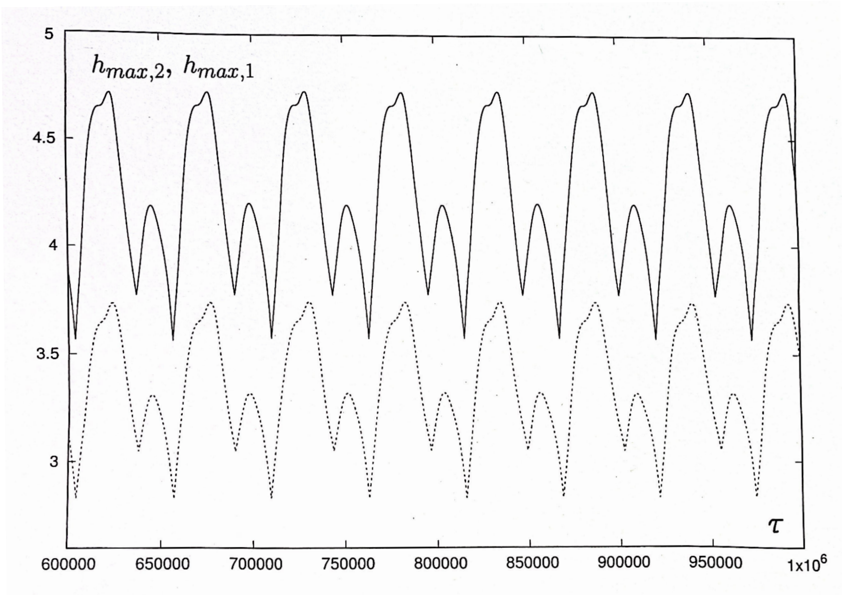

Figure 23. The oscillations of $h_{max,2}(\tau)$ (solid line) and $h_{max,1}(\tau)$ (dashed line) for $\bar{M} = -2.825$, $\Delta_X = 0.1$, $\Delta_Y = 0.25$, $Bo = 0$ and $Bi = 20$.

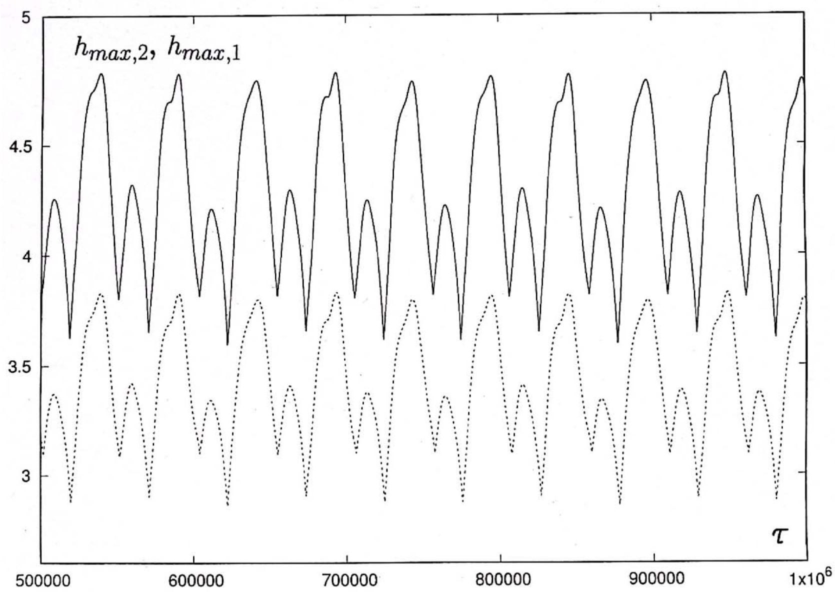

Figure 24. The oscillations of $h_{max,2}(\tau)$ (solid line) and $h_{max,1}(\tau)$ (dashed line) for $\bar{M} = -2.925$, $\Delta_X = 0.1$, $\Delta_Y = 0.25$, $Bo = 0$ and $Bi = 20$.

5. The Influence of Gravity on the Droplet Dynamics

Now, let us consider the action of gravity on the droplets. If we take the stationary droplet obtained under the action of the symmetric field $M(X, Y)$ ($\bar{M} = -2$, $\Delta_X = \Delta_Y = 0.1$) as the initial condition (see Figure 3), under the action of gravity ($Bo = 0.1$), the droplet is essentially flattened. The intermediate stages of the evolution of the initially round droplet are presented in Figure 25. Under the action of the thermocapillary flow in the substrate directed along the axis $Y = X$, the droplet changes its shape and height. The isolines and the shapes of the interfaces, corresponding to the final equilibrium state, are shown in Figures 26 and 27 (cf. Figures 3 and 26). The droplet still keeps the symmetry with respect to axis $Y = X$.

Under the action of gravity ($Bo = 0.05$) on the asymmetric stationary droplet shown in Figure 7 ($\bar{M} = -2$, $\Delta_X = 0.1$; $\Delta_Y = 0.5$), we obtain the asymmetric significantly flattened droplet (cf. Figures 7 and 28).

Let us take as initial conditions the periodic oscillations presented in Figures 19 and 20a. Under the action of sufficiently small gravity ($Bo = 0.01$), oscillations are suppressed and the steady droplet develops in the system. A snapshot of the fields of (a) $h_2(X, Y, \tau)$ and (b) $h_1(X, Y, \tau)$ is shown in Figure 29. The height of the droplet is essentially lower than that obtained in the absence of gravity (cf. Figures 20a and 29a).

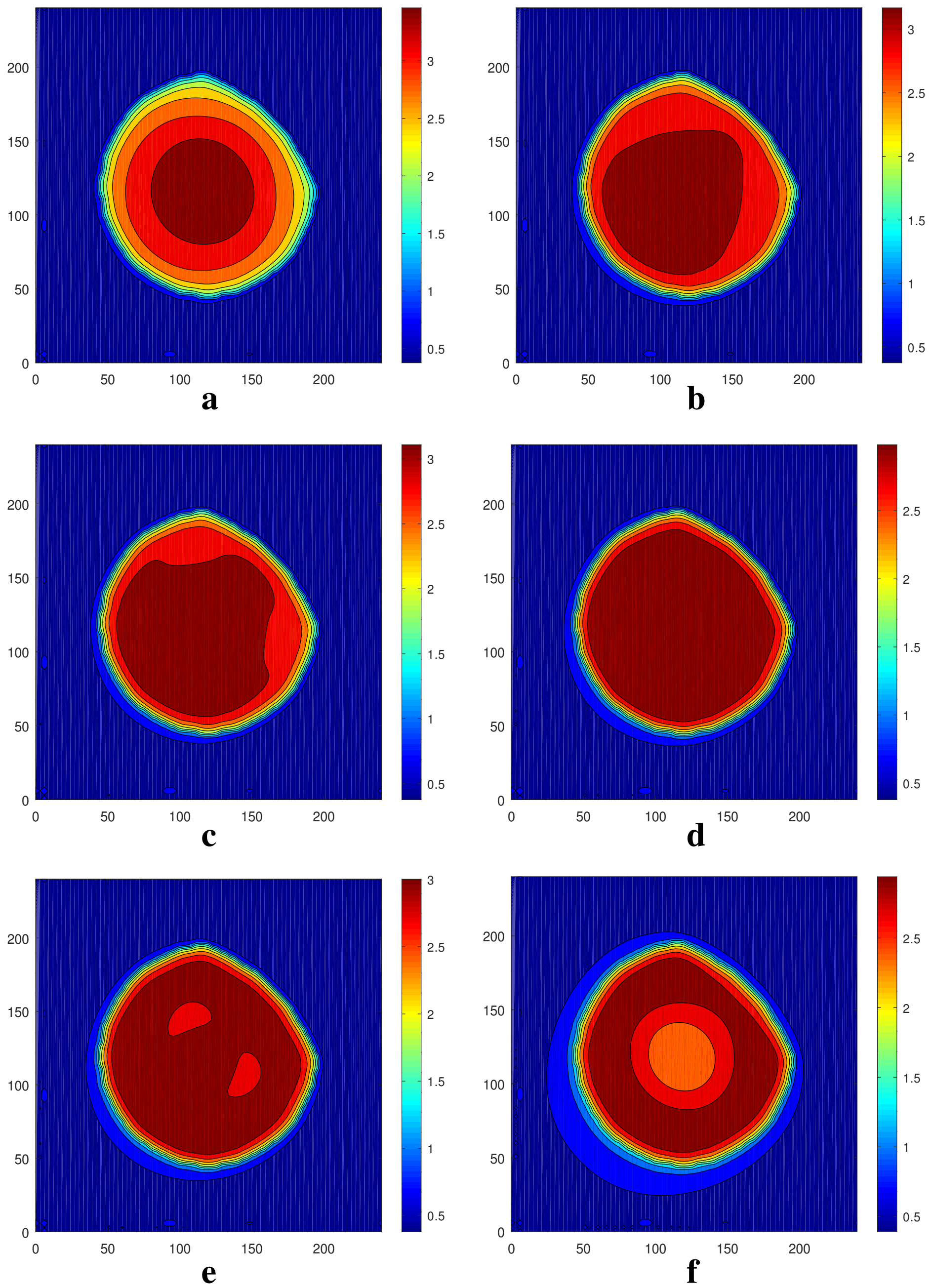

Figure 25. The fields of $h_2(X, Y, \tau)$ for $\bar{M} = -2$, $\Delta_X = \Delta_Y = 0.1$, $Bo = 0.1$ and $Bi = 20$: (**a**) $\tau = 250$; (**b**) $\tau = 450$; (**c**) $\tau = 500$; (**d**) $\tau = 650$; (**e**) $\tau = 850$ (**f**) $\tau = 2500$.

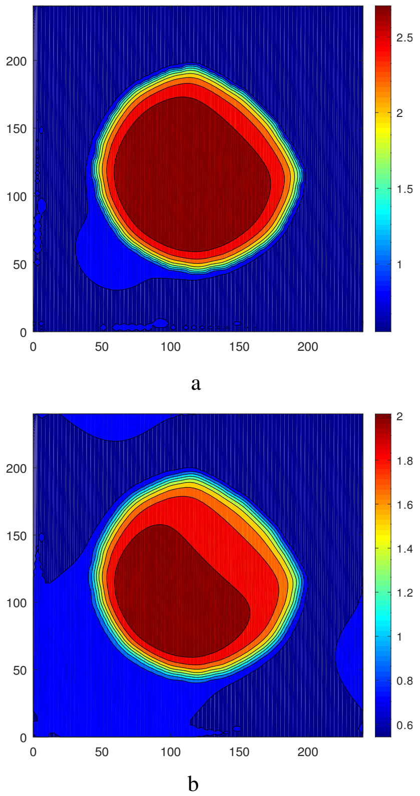

Figure 26. A snapshot of the fields of $h_2(X, Y, \tau)$ and $h_1(X, Y, \tau)$ for $\bar{M} = -2$, $\Delta_X = \Delta_Y = 0.1$, $Bo = 0.1$, $Bi = 20$ and $\tau = 1 \times 10^6$.

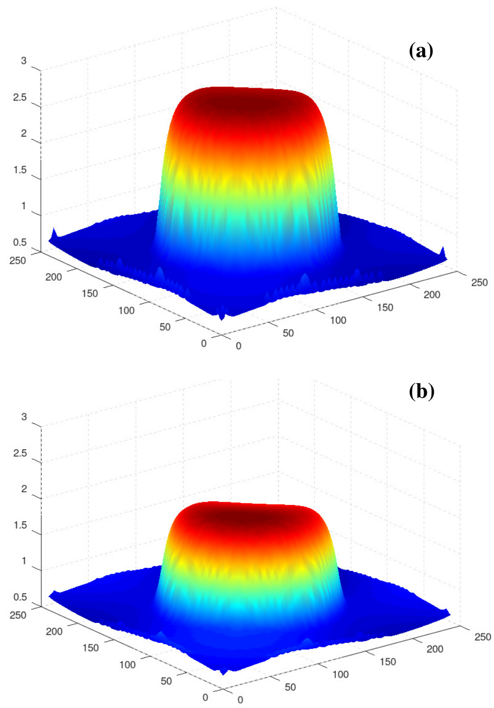

Figure 27. The shapes of (**a**) $h_2(X, Y, \tau)$ and (**b**) $h_1(X, Y, \tau)$ for $\bar{M} = -2$, $\Delta_X = \Delta_Y = 0.1$, $Bo = 0.1$, $Bi = 20$ and $\tau = 1 \times 10^6$.

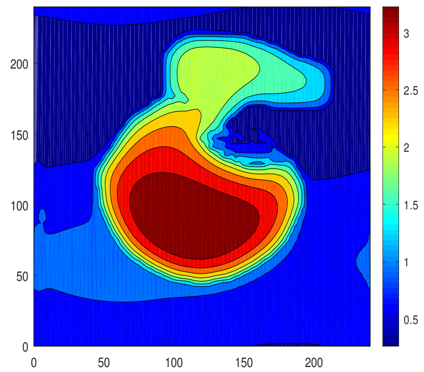

a

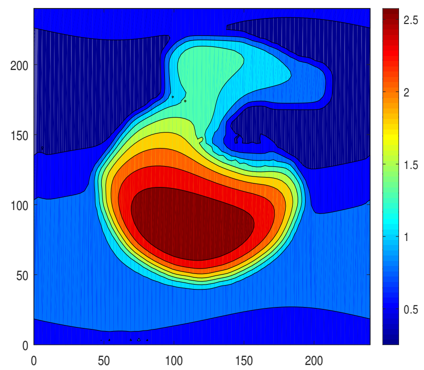

b

Figure 28. A snapshot of the fields of $h_2(X, Y, \tau)$ and $h_1(X, Y, \tau)$ for $\bar{M} = -2$, $\Delta_X = 0.1$, $\Delta_Y = 0.5$, $Bo = 0.05$, $Bi = 20$ and $\tau = 1 \times 10^6$.

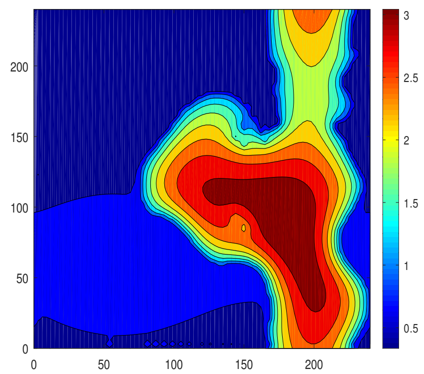

a

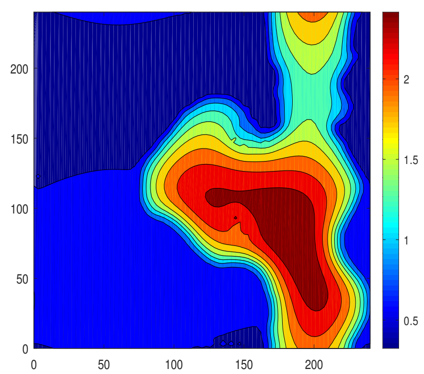

b

Figure 29. A snapshot of the fields of $h_2(X, Y, \tau)$ and $h_1(X, Y, \tau)$ for $\bar{M} = -2$, $\Delta_X = 0.1$, $\Delta_Y = 0.25$, $Bo = 0.01$, $Bi = 20$ and $\tau = 1 \times 10^6$.

6. The Influence of the Biot Number on the Shape of the Droplet

Let us consider the influence of the Biot number Bi on the shape of droplets. We take the stationary droplet obtained under the action of the symmetric field $M(X, Y)$ ($\bar{M} = -2$, $\Delta_X = \Delta_Y = 0.1$) as the initial conditions (see Figure 3). With a decrease in Bi, under the action of the thermocapillary flow in the substrate directed along the axis $Y = X$, the droplet is completely destroyed, and we obtain a square pattern. A snapshot of the field $h_2(X, Y, \tau)$, corresponding to the final equilibrium state for a sufficiently small value of Bi, is shown in Figure 30. The pattern keeps the symmetry with respect to axis $Y = X$. The shape of the upper interface is presented in Figure 31. The similar patterns generated by the bottom temperature modulation have been obtained in two-layer films [27].

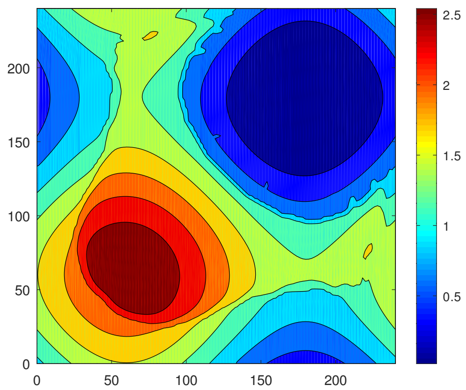

Figure 30. A snapshot of the field of $h_2(X, Y, \tau)$ for $\bar{M} = -2$, $\Delta_X = \Delta_Y = 0.1$, $Bo = 0$, $Bi = 0.1$ and $\tau = 1 \times 10^6$.

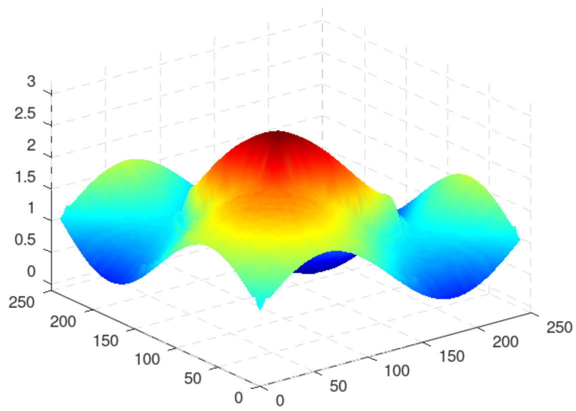

Figure 31. The shape of the interface $h_2(X, Y, \tau)$ for $\bar{M} = -2$, $\Delta_X = \Delta_Y = 0.1$, $Bo = 0$, $Bi = 0.1$ and $\tau = 1 \times 10^6$.

Let us note that the same steady regime has been obtained from the other initial conditions when a droplet of liquid 2 with a Gaussian shape was imposed on a flat layer of liquid 1.

The redistribution of the liquids in the droplet and in the substrate along the axis $Y = X$ with the maximum shifted to the region $X < L/2$ also takes place for sufficiently small values of $\bar{M}$ ($\bar{M} = -0.1$, $\Delta_X = \Delta_Y = 0.1$, $Bi = 0.5$). The intermediate stages of the evolution of the field $h_2(X, Y, \tau)$ at different instants of time are presented in Figure 32. A snapshot of the field $h_2(X, Y, \tau)$ and the corresponding shape of the upper interface at the final equilibrium state are shown in Figures 33 and 34.

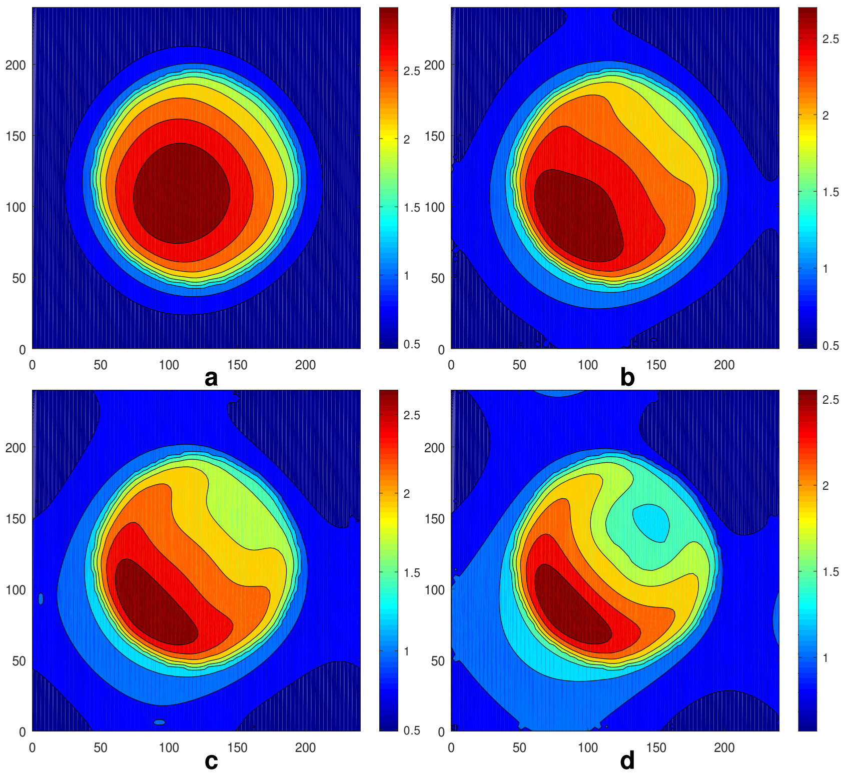

Figure 32. The fields of $h_2(X, Y, \tau)$ for $\bar{M} = -0.1$, $\Delta_X = \Delta_Y = 0.1$, $Bo = 0$ and $Bi = 0.5$: (**a**) $\tau = 10{,}000$: (**b**) $\tau = 25{,}000$; (**c**) $\tau = 40{,}000$; (**d**) $\tau = 80{,}000$.

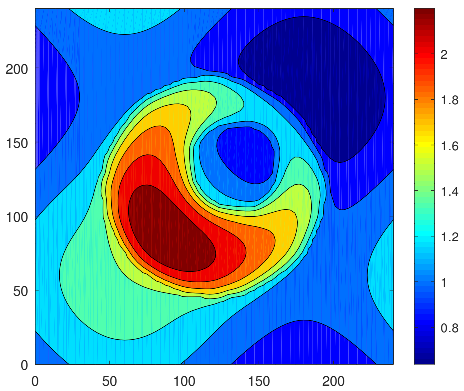

Figure 33. A snapshot of the field of $h_2(X, Y, \tau)$ for $\bar{M} = -0.1$, $\Delta_X = \Delta_Y = 0.1$, $Bo = 0$, $Bi = 0.5$ and $\tau = 1 \times 10^6$.

Now, let us take as initial conditions the periodic oscillations presented in Figures 19 and 20a. With a decrease in Bi (at $Bi \leq 18.95$), oscillations are suppressed and the steady asymmetric droplet develops in the system. A snapshot of the field of $h_1(X, Y, \tau)$ is shown in Figure 34. Let us note that the asymmetric droplet has also been obtained for sufficiently small values of $\bar{M}$ and Bi ($\bar{M} = -0.17$, $\Delta_X = 0.1$, $\Delta_Y = 0.25$, $Bi = 0.95$). The isolines and the shape of the upper interface, corresponding to the final equilibrium state, are shown in Figures 35 and 36. One can see that the symmetry with respect to axis $Y = X$ is broken.

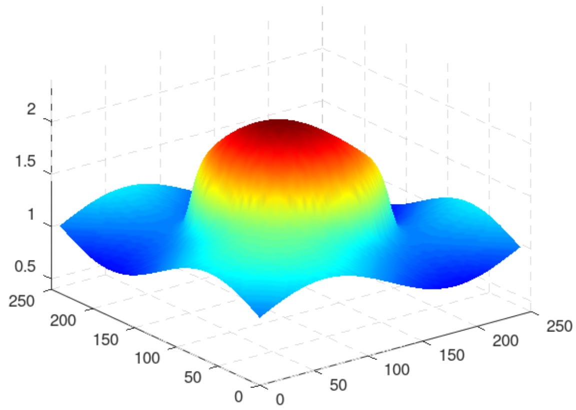

Figure 34. The shape of the interface $h_2(X, Y, \tau)$ for $\bar{M} = -0.1$, $\Delta_X = \Delta_Y = 0.1$, $Bo = 0$, $Bi = 0.5$ and $\tau = 1 \times 10^6$.

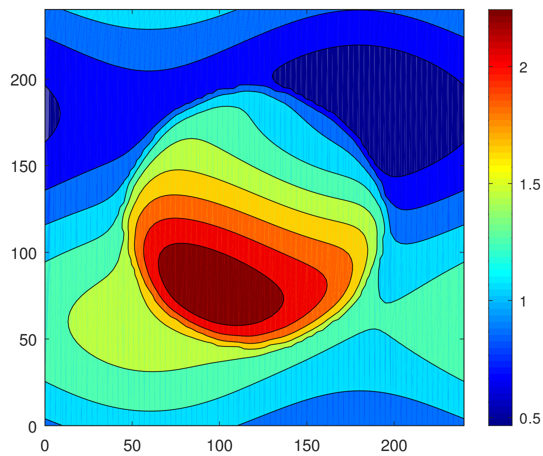

Figure 35. A snapshot of the field of $h_2(X, Y, \tau)$ for $\bar{M} = -0.17$, $\Delta_X = 0.1$, $\Delta_Y = 0.25$, $Bo = 0$, $Bi = 0.95$ and $\tau = 1 \times 10^6$.

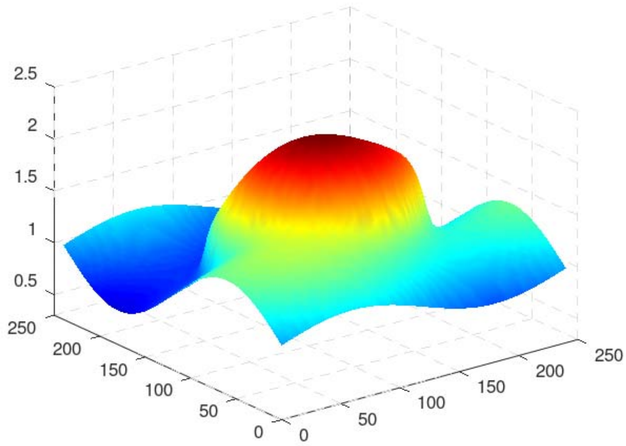

Figure 36. The shape of the interface $h_2(X, Y, \tau)$ for $\bar{M} = -0.17$, $\Delta_X = 0.1, \Delta_Y = 0.25$, $Bo = 0$, $Bi = 0.95$ and $\tau = 1 \times 10^6$.

7. Conclusions

The dynamics of a droplet on a liquid substrate in the case of an inhomogeneous cooling from below has been investigated. The problem is studied numerically in the framework of the longwave approximation and the precursor model.

It is shown that a two-dimensional spatial inhomogeneity of the substrate temperature creates more diverse flow regimes than a one-dimensional temperature inhomogeneity.

The nonhomogeneous cooling creates a disbalance of thermocapillary stresses that leads to the redistribution of the liquids in the droplet and in the substrate. It is found that the droplet can be stationary or subject to oscillations caused by an oscillatory Marangoni instability. The two-dimensional spatial inhomogeneity of the temperature enhances the oscillatory instability threshold, and it can *suppress* oscillations, leading to the formation of steady droplets. In a definite region of parameters, the two-dimensional spatial modulation can lead to the *excitation* of the specific type of periodic oscillations with different adjacent maxima. A diagram of regimes in the plane (δ_X, δ_Y) has been constructed. The bistability in several points has been obtained. The gravity flattens the droplet and suppresses oscillations.

The influence of the Biot number on the shape of the droplet has been studied. The smaller the Bi, the stronger the inhomogeneities of the temperature on the free surface and, thus, the stronger the action of the thermocapillary effect. Square patterns similar to those generated by the bottom temperature modulation in two-layer films have been obtained.

Author Contributions: A.N. and I.S. wrote the paper together. All authors have read and agreed to the published version of the manuscript

Funding: This research was supported by the Israel Science Foundation (grant No. 843/18).

Data Availability Statement: Data are contained within the article.

Conflicts of Interest: The authors declare no conflict of interest.

References

1. de Gennes, P.G. Wetting: Statics and dynamics. *Rev. Mod. Phys.* **1985**, *57*, 827. [CrossRef]
2. de Gennes, P.G.; Brochard-Wyart, F.; Quérxex, D. *Capillarity and Wetting Phenomena: Drops, Bubbles, Pearls, Waves*; Springer: Berlin/Heidelberg, Germany, 2004.
3. Labanieh, L.; Nguyen, T.N.; Zhao, W.A.; Kang, D.K. Floating droplet array: An ultrahigh-throughput device for droplet trapping, real time analysis and recovery. *Micromachines* **2015**, *60*, 1469–1482. [CrossRef] [PubMed]
4. Yamini, Y.; Rezazadeh, M.; Seidi, S. Liquid-phase microextraction—The different principles and configurations. *TRAC—Trends Anal. Chem.* **2019**, *112*, 264–272. [CrossRef]
5. Ju, G.; Yang, X.; Li, L.; Cheng, M.; Shi, F. Removal of oil spills through a self-propelled smart device. *Chem. Asian J.* **2019**, *14*, 2435–2439. [CrossRef] [PubMed]
6. Rybalko, S.; Magome, N.; Yoshikawa, K. Forward and backward laser-guided motion of an oil droplet. *Phys. Rev. E* **2004**, *70*, 046301. [CrossRef] [PubMed]
7. Song, C.; Moon, J.K.; Lee, K.; Kim, K.; Pak, H.K. Breathing, crawling, budding, and splitting of a liquid droplet under laser heating. *Soft Matter* **2014**, *10*, 2679–2684. [CrossRef] [PubMed]
8. Buffone, C. Formation, stability and hydrothermal waves in evaporating liquid lenses. *Soft Matter* **2019**, *15*, 1970–1978. [CrossRef]
9. Nepomnyashchy, A.; Simanovskii, I. Droplets on the liquid substrate: Thermocapillary oscillatory instability. *Phys. Rev. Fluids* **2021**, *6*, 034001. [CrossRef]
10. Nepomnyashchy, A.A.; Simanovskii, I.B. Marangoni instability in ultrathin two-layer films. *Phys. Fluids* **2007**, *19*, 122103. [CrossRef]
11. Greco, E.F.; Grigoriev, R.O. Thermocapillary migration of interfacial droplets. *Phys. Fluids* **2009**, *21*, 042105. [CrossRef]
12. Yakshi-Tafti, E.; Cho, H.J.; Kumar, R. Droplet actuation on a liquid layer due to thermocapillary motion: Shape effect. *Appl. Phys. Lett.* **2010**, *96*, 264101. [CrossRef]
13. Keiser, L.; Bense, H.; Colinet, P.; Bico, J.; Reyssat, E. Marangoni bursting: evaporation induced emulsification of binary mixtures on a liquid layer. *Phys. Rev. Lett.* **2017**, *118*, 074504. [CrossRef]
14. Neumann, F. *Vorlesungen über die Theorie der Capllarität*; Teubner: Leipzig, Germany, 1894.
15. Kriegsmann, J.J.; Miksis, M.J. Steady motion of a drop along a liquid interface. *SIAM J. Appl. Math.* **2003**, *64*, 18. [CrossRef]
16. Craster, R.V.; Matar, O.K. On the dynamics of liquid lenses. *J. Colloid Interface Sci.* **2006**, *303*, 503–516. [CrossRef] [PubMed]
17. Pototsky, A.; Bestehorn, M.; Merkt, D.; Thiele, U. Morphology changes in the evolution of liquid two-layer films. *J. Chem. Phys.* **2005**, *122*, 224711. [CrossRef] [PubMed]
18. Nepomnyashchy, A.A.; Simanovskii, I.B. Effect of gravity on the dynamics of non-isothermic ultra-thin two-layer films. *J. Fluid Mech.* **2010**, *661*, 1–31. [CrossRef]
19. Nepomnyashchy, A.; Simanovskii, I. Nonlinear Marangoni waves in a two-layer film in the presence of gravity. *Phys. Fluids* **2012**, *24*, 032101. [CrossRef]
20. Oron, A.; Davis, S.H.; Bankoff, S.G. Long-scale evolution of thin liquid films. *Rev. Mod. Phys.* **1997**, *69*, 931. [CrossRef]

21. Pototsky, A.; Oron, A.; Bestehorn, M. Vibration-induced flotation of a heavy liquid drop on a lighter liquid film. *Phys. Fluids* **2019**, *31*, 087101. [CrossRef]
22. Sternling, C.V.; Scriven, L.E. On cellular convection driven by surface tension gradients: Effects of mean surface tension and surface viscosity. *J. Fluid Mech.* **1964**, *19*, 321–340.
23. Géoris, P.; Hennenberg, M.; Lebon, G.; Legros, J.C. Investigation of thermocapillary convection in a three-liquid-layer systems. *J. Fluid Mech.* **1999**, *389*, 209–228. [CrossRef]
24. Princen, H.M. Shape of interfaces, drops, and bubbles. In *Surface and Colloid Science*; Matijevic, E., Ed.; Wiley: New York, NY, USA, 1969; Volume 2, p. 1.
25. Nepomnyashchy, A.; Simanovskii, I. Marangoni instabilities of droplets on the liquid substrate under the action of a spatial temperature modulation. *J. Fluid Mech.* **2022**, *936*, A26. [CrossRef]
26. Nepomnyashchy, A.; Simanovskii, I.; Legros, J.C. *Interfacial Convection in Multilayer Systems*, 2nd ed.; Springer: New York, NY, USA, 2012.
27. Nepomnyashchy, A.; Simanovskii, I. The influence of two-dimensional temperature modulation on nonlinear Marangoni waves in two-layer films. *J. Fluid Mech.* **2018**, *846*, 944–965. [CrossRef]